Title: Sodium sensing in neurons with a dendrimer-based nanoprobe.

Authors: Lamy CM, Sallin O, Loussert C, Chatton JY

Journal: ACS nano

Year: 2012 Feb 28

Issue: 6

Volume: 2

Pages: 1176-87

DOI: 10.1021/nn203822t

ACS Nano (2012) 6(2) · 1176–1187

Sodium sensing in neurons with a dendrimer-based nanoprobe

Christophe Lamy[1,*], Olivier Sallin[2], Céline Loussert[3] and Jean-Yves Chatton[1,2]

[1] Department of Cell Biology and Morphology, University of Lausanne, Switzerland

[2] Cellular Imaging Facility, University of Lausanne, Switzerland

[3] Electron Microscopy Facility, University of Lausanne, Switzerland

* Corresponding author:

Christophe Lamy

Dept. of Cell Biology and Morphology

University of Lausanne

Rue du Bugnon 9

CH-1005 Lausanne

Switzerland

Tel. +41-21-692-5117

Fax. +41-21-692-5105

E-mail: christophe.lamy@unil.ch

Abstract

Ion imaging is a powerful methodology to assess fundamental biological processes in live cells. The limited efficiency of some ion-sensing probes and their fast leakage from cells are important restrictions to this approach. In this study we present a novel strategy to perform prolonged fluorescence imaging of intracellular ion dynamics with dendrimer-based nanoprobes. A new sodium sensitive nanoprobe was generated by encapsulating a fluorescent dye in a PAMAM dendrimer nanocontainer. This nanoprobe is very stable and has high sodium sensitivity and selectivity. When loaded in neurons in live brain tissue, it homogenously fills the entire cell volume, including small processes, and stays for long durations, with no detectable alterations of cell functional properties. We demonstrate the suitability of this new sodium nanosensor for reliable monitoring of physiological sodium responses during neuronal activity.

Keywords

PAMAM dendrimer, nanoprobe, fluorescence imaging, neuron, sodium

Introduction

Fluorescence imaging is widely used in biomedical sciences for a large spectrum of applications ranging from the morphological analysis of anatomical structures to time-resolved measurements of intracellular molecular events [1, 2]. It enables non invasive probing of biological processes with high spatial resolution in ex-vivo tissue preparations as well as in whole organisms [3, 4]. A powerful application of this technique is the ability to monitor in real-time the complex intracellular fluxes of ions and metabolites that underlie many essential physiological functions [5, 6]. Most studies so far focused mainly on imaging Ca^{2+} as a ubiquitous secondary signal giving large amplitude, easily detectable responses. Other key cellular ions such as Na^+, K^+ and Cl^- that give more elusive responses proved more difficult to measure [7-10]. As a result, detailed knowledge of their temporal and spatial dynamics is still largely missing. Sodium imaging in particular is an attractive way of assessing many fundamental cellular processes, from the transport of small molecules through epithelial barriers to the integration of complex signals in the brain, that depend on the transmembrane Na^+ gradient. Unlike Ca^{2+} signals, Na^+ changes are a more direct reflection of primary cellular mechanisms and their measurement is not hampered by buffering of responses by cytosolic proteins or by the indicator itself [4, 11]. However, the poor characteristics of available Na^+ probes have rendered Na^+ imaging an uneasy task [8, 12].

Making good fluorescent probes for live imaging is quite challenging. Requirements for an ideal ion-sensitive molecule are: excitation with visible or near-infrared light, a safe delivery to cells, targeting to the appropriate sub-cellular compartment, absence of cell leakage or photobleaching, absence of interaction with cellular physiology, absence of cytotoxicity, high selectivity to the ion species studied, affinity for the target in the physiological range, high brightness and large fluorescence changes during physiological responses (For review, see Johnson [13]). Most existing ion-sensitive sensors are small fluorescent dyes. These dyes might provide bright homogeneous signal but do not remain in cells for long durations. They can also be difficult to load into specific cell types. Advances in genetic engineering enabled the generation of ion-sensitive genetically-encoded fluorescent proteins. Unlike fluorescent dyes they can be targeted to specific cells or cellular sub-compartments and enable long term imaging. Unfortunately they are only available for a small set of ions and metabolites and usually give weaker signals in physiological conditions than fluorescent dyes [14, 15].

More recently, fluorescent nanoprobes were developed and used for fluorescence microscopy. These include quantum dots, silicon and carbon nanoparticles, nanophosphors and gold-silver nanocages [16-22]. Nanoparticles usually provide bright and stable signal over time. They can remain in cells for days or longer [20]. However they are not intrinsically sensitive to ion-concentrations and need further engineering to obtain fluorescent ion sensors. Quantum dots-based K^+, Cl^- and pH-sensitive sensors have been reported [23-26]. Similarly, a very elegant approach was used to make a Na^+ nanosensor by embedding a quantum dot in an ion-selective polymer containing a pH indicator. This sensor showed good Na^+ sensitivity and selectivity in vitro, but its Na^+ responsiveness was not demonstrated in live cell yet [27]. Na^+ nanosensors made of a polymer-ionophore-chromoionophore combination without quantum dots were also devised and proved to detect efficiently Na^+ transients in cultured cells [28-31]. An important disadvantage of these nanoprobes is their large size, typically over 100 nm in diameter, which is likely to limit their diffusion in smaller cell compartments, such as axons and dendrites of neurons, were most of the cell's biological activity is often concentrated. In addition, their loading often requires invasive procedures like picoinjection or biolistic delivery that can damage living cells. Nanoparticles are also frequently toxic unless a specific biocompatible coating is added and even then they can lead to adverse effects on cell viability like cell blebbing [29, 32]. Finally, they can be unstable in biological solutions with risks of aggregation and of reduced lifetime due to component leaching [28, 29, 31].

We thought to use dendrimers to generate a new type of Na^+ nanosensor that would overcome the limitations of currently existing Na^+-sensitive nanoprobes and Na^+ dyes. Dendrimers are branched polymers with well defined sizes and geometry. After several layers of branching they make spheres that contain solvent-filled cavities. These structural features endow them with the ability to encapsulate small guest molecules and act as nanocontainers. Dendrimer nanocontainers have been extensively used for drug and gene delivery applications [33-35]. Efficient encapsulation of fluorescent dyes by dendrimers has also been reported [36, 37]. However, this property has not been used in molecular imaging yet. In this study we tested whether a Na^+ dye could be encapsulated in a dendrimer in order to prolong its intracellular half-life while maintaining its Na^+ response characteristics. We also assessed whether a Na^+ nanoprobe built on this principle could be used to probe cell functions in thick tissue preparations without disturbing baseline physiological parameters.

Results and discussion

We generated Na^+ sensing nanoprobes using Tomalia-type poly(amidoamine) (PAMAM) dendrimers [34, 35, 38] doped with Na^+ sensitive dyes CoroNa Green (CG) and CoroNa Red (CR). We choose generation 4.5 or 5 (G4.5-G5) dendrimers to take advantage of the nanocontainer property of the nanoparticle and enable encapsulation of the guest fluorescent dye while maintaining a good communication of the dendritic cavity with the external medium. PAMAM dendrimers smaller than G3 do not allow encapsulation whereas for generations higher than G6 surface congestion impairs access to the dendrimer interior [35]. Three Na^+ nanosensors designs were tested. CG was combined with G5 dendrimers carrying either an amidoamine (PAMAM-NH_2-CG) or a poly(ethyleneglycol) (PAMAM-PEG-CG, Fig. 1A) surface. CR, a positively charged molecule, was used in conjunction with a G4.5 dendrimer functionalized with a sodium carboxylate surface (PAMAM-COONa-CR). We used a limiting dye:dendrimer ratio of 1.2 in order to avoid having multiple dye molecules associated with the same dendrimer particle, that could result in self-quenching of the fluorescence [39, 40]. To demonstrate the stability of these complexes, we performed exhaustive ultrafiltration with a 3 kDa cut-off membrane allowing the separation of complexes (~30,000 - 100,000 Da) and host (~600 Da). After 4 rounds of washing with HEPES buffer, the complexes were retained in the filtration cell while the unbound dye molecules were collected in the flow-through and quantified by UV-Vis spectrometry. The bound fraction of the dye was found to be 68.3% for PAMAM-PEG-CG, 91.3% for PAMAM-NH_2-CG and 100% for PAMAM-COONa-CR. The final dye:dendrimer stoichiometry was therefore 0.82 for PAMAM-PEG-CG, 1.10 for PAMAM-NH_2-CG and 1.20 for PAMAM-COO-CR.

The different dye binding capacity of PAMAM-PEG-CG and PAMAM-NH_2-CG indicates a different mode of complexation of the dye with host dendrimers. We performed further measurements to gain insight on this interaction. Organic acids were shown to be preferentially retained in the inner cavities of water-soluble dendrimer cavities as a result of electrostatic interactions with internal tertiary amines [41-44]. Tertiary amines in the PAMAM dendrimer core are known to be more acid than the primary amine groups in the periphery (pKa = 6.65 and 9.20, respectively [43]). At pH 7.4, most of the surface primary amines are positively charged while 85% of interior amine groups are uncharged. We did an acid-base titration of free CG and obtained a pKa of 5.04, meaning that in our conditions almost all CG molecules are negatively charged. In

PAMAM-NH_2-CG, CG is thus likely to mainly interact with the surface amines. In PAMAM-PEG-CG, the outer shell of PEG is electroneutral and does not offer strong enough interactions to stabilize the dye on the nanoprobe. To check if the affinity of PAMAM-PEG for CG is related to acid-base interactions, we prepared a batch of PAMAM-PEG-CG nanoprobe at pH 6. In this condition, the binding capacity of the dendrimer should become higher as the number of protonated internal amines increase while CG remains largely deprotonated. After ultrafiltration, the dye bound fraction increased to 78.3%, demonstrating that electrostatic interactions are important for the retention of CG. We then used fluorescence anisotropy, reflecting the rotational freedom of fluorescent molecules, as a way to probe the host-guest interaction [37]. Steady-state fluorescence anisotropy values were found to be significantly higher for PAMAM-PEG-CG ($r=0.208\pm0.002$, $p=0.0001$) and PAMAM-NH_2-CG ($r=0.145\pm0.004$, $p=0.0004$) than for free CG ($r=0.116\pm0.003$), confirming that CG is closely associated with the nanoparticles. These measurements indicated that anisotropy was significantly higher for PAMAM-PEG-CG than for PAMAM-NH_2-CG ($p=0.0001$). This result is compatible with CG being entrapped in the dendrimer cavity of PAMAM-PEG [45], resulting in a greater reduction in rotational freedom than in the case of PAMAM-NH_2-CG where the dye is thought to be primarily associated with the shell terminal amines.

To assess whether the association with the dendrimer would alter the dyes' spectral properties, we acquired the fluorescence emission spectra of the three nanoprobes and of the corresponding free dyes in vitro in a buffer having a similar ionic strength and pH as the intracellular environment. The emission spectra PAMAM-NH_2-CG and PAMAM-COONa-CR were identical to the emission spectra of free CG and CR respectively (Fig. 1B). In contrast, the emission spectrum of PAMAM-PEG-CG showed a bathochromic shift in the wavelength of the emission maximum of 12 nm as compared to free CG (Fig. 1B). This shift is an indication of a complex formation between the dendrimer host and the dye guest as was previously reported for other anionic dyes such as Rose Bengal and tetrachlorofluorescein [41]. To confirm this complexation, we measured the absorption spectra of free CG and PAMAM-PEG-CG. Similarly to fluorescence emission, we observed a 12 nm bathochromic shift in the wavelength of the absorption maximum with the nanoprobe (Fig. S1). These spectra were measured on dendrimer-dye complexes after the removal of unbound dye by ultrafiltration. Similar full width at half maximum values show that the spectra of the complexes are not altered by the presence of

contaminating free dye. In addition, spectra of the PAMAM-PEG-CG nanoprobe generated more than a month later were unchanged, showing that there is no significant dye leaching from the complexes, and that the fluorescent nanoprobe preparations were stable.

We then tested the performance of our nanoprobes to measure Na^+. We recorded the fluorescence emission spectra of dyes and of dye-dendrimer complexes in buffers containing graded Na^+ concentrations (Fig. 2A,B). Fluorescence intensity of all nanoprobes increased with $[Na^+]$. Peak amplitudes of spectra were plotted against $[Na^+]$. Except for PAMAM-COONa-CR, the relationship between $[Na^+]$ and normalized changes in fluorescence showed remarkable linearity in the physiologically relevant 0-50 mM Na^+ range (Fig. 2B). Na^+ sensitivity was higher for PAMAM-PEG-CG than for free CG. This interesting property might be due to restricted movements inside the cavity, resulting in reduced non-radiative relaxation and an increased fluorescence lifetime [45, 46]. Differences in the local nanoenvironment polarity as compared to the bulk solution and reduction of concentration quenching due to a larger distance between fluorescent molecules could also contribute to this increased fluorescent response [46, 47]. PAMAM-NH_2-CG was less sensitive to Na^+ than both PAMAM-PEG-CG and free CG. We attribute this observation to the repulsion of Na^+ by the positively charged surface of PAMAM-NH_2 [48]. PAMAM-COONa-CR had the poorest Na^+ response curve. This could be explained by the quenching of CR fluorescence and the local buffering of Na^+ by PAMAM-COONa surface carboxylate groups [49, 50]. Since PAMAM-PEG-CG gave the best responses to Na^+, we decided to focus on this nanoprobe for the remaining of the study.

A concern with measuring cytosolic Na^+ is the possible interference of simultaneously varying concentrations of other intracellular ions. The main cytosolic monovalent cation is K^+. We tested the sensitivity of PAMAM-PEG-CG to K^+ and found no significant effect over a large concentration range (R^2=-0.298, p=0.794, Fig. 2C). Intracellular pH can also vary during cellular activation and affect the efficiency of fluorescent probes. PAMAM-PEG-CG was not significantly influenced by pH in a physiological range (R^2=0.445, p=0.206, Fig. 2D).

The properties of the Na^+ nanosensor were further studied in the intracellular environment. PAMAM-PEG-CG was loaded in a glass pipette and delivered to live neurons in acute neocortical brain slices by single-cell electroporation (Fig. 3A). This method was shown to be a safe way to deliver charged macromolecules to neurons [51]. We used this approach instead of whole-cell patch-clamp to avoid altering Na^+ responses by dilution with the pipette solution [8, 52].

With this technique we were able to specifically target the nanoprobe to selected cells (Fig. 3B). We could also sequentially fill multiple cells if needed (Fig. 3C). The nanoprobe diffused rapidly through the entire cell volume including to dendrites and the axon (Fig. 3B), indicating that the size of the nanoparticle is not an obstacle for imaging remote small cellular compartments. The size of PAMAM-PEG-CG nanoparticles was measured by transmission electron microscopy (TEM) using uranyl acetate as a contrast agent (Fig. 4). The average particle diameter measured from TEM images was 6.57±0.04 nm (n=1785 particles). This size is in agreement with the diameter of 6.5 nm estimated from average C-C and C-N bonds lengths and with the sizes measured with other techniques for G5 dendrimers [53-56]. PAMAM-PEG-CG nanoparticles are thus much smaller than previously published Na^+ nanosensors [28, 30, 31]. Those gave less homogeneous patterns of fluorescence than the one we observed, probably due to the larger volume and more inhomogeneous shape of the probes, leading to some degree of intracellular clustering.

The main reason for devising a CG-doped nanoparticle instead of using CG alone was the extremely fast leakage of this dye from living cells. PAMAM-PEG-CG intracellular fluorescence baseline in slice neurons was stable over the duration of experiments (typically more than one hour), in sharp contrast with the fast decay of CG fluorescence (Fig. 3D). The slow residual decay in fluorescence is likely due to CG photobleaching as indicated by its faster rate when laser illumination was increased. Previously described nanoprobes suffered from component leaching [28, 29, 31]. If this were the case with PAMAM-PEG-CG, unbound CG would exit from cells very fast after the loading of the nanoprobe. This would lead to a rapid initial drop in fluorescence, which we did not observe. Furthermore, the fact that the same batch of nanoprobe could be used over weeks without any significant leakage indicates that there is no dye leaching from the probe, confirming the stability observed in vitro.

A frequent concern with nanoparticles is their cytotoxicity [35]. We addressed this issue by recording the functional properties of neurons using whole-cell electrophysiology. Passive membrane properties, cell excitability and action potential characteristics were identical in neurons filled with PAMAM-PEG-CG and control neurons (Table 1). These data indicate that our dendrimer-based nanosensor does not affect essential cell functions. It is noteworthy that Na^+-dependent electrical responses like action potentials were unaffected, ruling-out any interference of the nanosensor with the measured parameter. Since neurons are extremely

sensitive to any modification of their internal environment, we can safely extrapolate that PAMAM-PEG-CG will be harmless to most other cell types. Innocuousness of this nanoprobe is attributable to the external coating with PEG, a functional group previously shown to increase biocompatibility[57, 58]. In our experience, dendrimers with charged surfaces, like PAMAM-NH_2 and PAMAM-COONa, induced microscopic alterations to cells reminiscent of the cell blebbing occasionally observed with other nanoparticles [29]. We conclude from these characteristics that our Na^+ nanoprobe is suitable for safe long term imaging of Na^+ responses in live cells.

Measurements of physiological Na^+ responses were performed in brain slices in layer 2/3 neocortical neurons loaded with PAMAM-PEG-CG as described earlier. We first induced neuronal Na^+ responses by local application of the excitatory neurotransmitter glutamate. Short puffs of glutamate (10-250 ms) delivered in the vicinity of a PAMAM-PEG-CG-filled neuron produced somatic Na^+ transients (Fig. 5A). The amplitude of Na^+ transients increased monotonically with the number of applied puffs (R^2=0.993, n=4 cells, Fig. 5B). Glutamate responses were abolished by the ionotropic glutamate AMPA receptor antagonist CNQX, confirming that they are due to Na^+ entry through Na^+-permeable AMPA receptors. These results demonstrate that our nanoprobe enables quantitative Na^+ measurements in live tissue preparations. Neuronal electrical activity always proved difficult to measure with Na^+ dyes, often requiring averaging multiple trials to reveal responses [52]. To investigate the efficiency of our nanoprobe, we checked whether we could detect Na^+ changes associated with the generation of action potentials. We stimulated afferent nerve fibers with a bipolar electrode placed in neocortical layer 4, 200 μm below the neuron filled with the sensor. This stimulation procedure was shown to induce consistent neuronal electrical responses. Repeated brief electrical pulses induced detectable single-trial somatic Na^+ transients (Fig. 5C). As expected, their size was much smaller than during pharmacological activation of AMPA receptors, nonetheless it increased with the amount of stimulation (Fig. 5C). There was a positive correlation between the number of stimuli and time integrated responses (R^2=0.761, n=9 trials, Fig. 5D). Electrically-induced Na^+ responses are usually larger in small cell compartments than in the soma, due to the slower diffusion of Na^+ [52]. We measured evoked Na^+ transients in basolateral dendrites. The amplitude of responses was found to be one order of magnitude larger in dendrites than in the soma (Fig. 5E). Na^+ channel blocker tetrodotoxin (TTX) inhibited evoked dendritic Na^+

responses (Fig 5E, lower trace). This shows that fluorescent transients we measured in neurons are selective Na^+ responses.

Collectively, these data indicate that PAMAM-PEG-CG is an efficient Na^+ nanosensor that can be used for the real-time detection of cytosolic Na^+ transients in live tissue during physiological activity. Sensitivity of the nanoprobe was 3.3 % fluorescence change/mM (%ΔF/F/mM), similar to free CG (3.2 %ΔF/F/mM) and to existing PEBBLE Na^+ nanosensor (2.7 %ΔF/F/mM [27]), but lower than quantum dot-based nanosensor (12.5 %ΔF/F/mM [27]). The linear dependence of the probe's response for $[Na^+]$ values observed during physiological activity indicate that PAMAM-PEG-CG can be used for quantitative $[Na^+]$ measurements [52]. A matter of concern is whether the probe truly reflects the bulk intracellular $[Na^+]$ or only the local $[Na^+]$ in the dendrimer internal environment. It has been shown that G5 dendrimer cavities are filled with the solvent and ions and that there is a dynamic exchange with the bulk solution [59]. Nonetheless, the positively charged interior of the dendrimer could repel Na^+ and lead to a distortion in $[Na^+]$ read-out similarly to the effect produced by surface charges [48]. However, the calibration curve we generated and the successful quantitative measurements of fast intracellular Na^+ changes demonstrate that this is not the case. The likely reason is that the positive charge density in the cavity is much lower at pH 7.4 than the charge density shown to create an unfavorable local nanoenvironment at the surface. Altogether, this nanoprobe is a sensible alternative to existing Na^+ dyes. Sodium imaging has relied so far mainly on fluorescent dye sodium-binding benzofuran isophtalate (SBFI [7]). This compound requires UV excitation which is suboptimal for imaging deep in tissue due to the strong scattering of UV photons and results in phototoxic damage [60]. Attempts to generate better Na^+ dyes produced several candidates. Sodium Green was one noticeable alternative [61] but it produced inaccurate Na^+ measurements due to interactions with cell proteins [12]. CoroNa Green, used in the present study, was another promising attempt but it suffered from a fast efflux from cells after loading [8, 29]. We show that combining CoroNa Green with a dendrimer does not alter the dye's Na^+ sensitivity and results in a vastly improved intracellular lifetime of the probe.

In conclusion, we present a novel strategy to produce ion-sensitive nanosensors based on the use of dendrimers. In addition to their characterization in vitro, we provide the first demonstration, to our knowledge, of the use such nanoprobes in neurons in whole-tissue preparations. These

sensors display a high ion responsiveness and biocompatibility and enable prolonged imaging of intracellular ion dynamics. This research led to the generation of a novel fluorescent nanosensor for markedly improved Na^+ imaging, especially well suited for real-time studies of physiological responses in live tissue samples and *in vivo* brain imaging. In addition, as these nanoprobes are straightforward to generate and stable over time, they could become an attractive tool for biologists.

Methods

Nanoprobe synthesis

CoroNa Green, Corona Red (Invitrogen, Carlsbad, USA) and PAMAM dendrimers (Dendritic Nanotechnologies Inc., Mount Pleasant, MI, USA) stock solutions were made in methanol (MeOH). G5 PAMAM dendrimers with 1,4-diaminobutane core and either amidoamine (29 kDa, 1 eq.) or poly(ethyleneglycol) methyl ether surface (104 kDa, 1 eq.) were stirred with 1.2 equivalents of CG (0.48 mM) at room temperature for 30 min. To probe the role of electrostatic interactions in the complexation of the dye, a batch of PAMAM-PEG-CG was prepared at pH 6.0. G4.5 PAMAM dendrimer with 1,4-diaminobutane core and sodium carboxylic surface (0.24 μmol, 10 wt.%, 1 eq.) was stirred with 1.2 equivalents of CR at room temperature for 30 min. An equal volume of Hepes buffer (10 mM, pH 7.4, HB) was added. pH was adjusted if necessary by addition of HCl. The mixture was stirred uncovered overnight to allow slow evaporation of MeOH. Remaining MeOH was evaporated under reduced pressure for 2h30 at 30°C. The preparation was resuspended in HB and ultrafiltered with a 3 kDa cut-off membrane (Millipore, Billerica, MA, USA). This procedure was repeated 4 times to ensure all unbound dye was removed. The flow-through was collected for quantification of the fraction of the dye associated with the dendrimer. Dendrimer-dye complexes retained on the ultrafiltration membrane were resuspended in HB at a concentration equivalent to 1 mM of the dye. They were filtered with a 0.22 μm filter to remove aggregates and stored at -20°C until used. All manipulations and storage were done in the dark to avoid photobleaching of the dye. Under these conditions, nanoprobes remained stable for many months.

UV-Vis spectrometry

UV-Vis absorbance spectra of fluorescent probes and optical density measurements were measured on a Nanodrop 1000 spectrophotometer (Thermo Fisher Scientific Inc., Waltham, MA, USA) in 1 μl volume. Quantifications of unbound dye concentration in ultrafiltration flow-through were done using the Beer-Lambert law with molar extinction coefficients of 68,000 M^{-1} cm^{-1} for CG and 92,000 M^{-1} cm^{-1} for CR.

Acid-base titration

Determination of the pKa of CG pKa was done by a spectrophotometric method, taking advantage of the different absorbance of protonated and deprotonated forms of CG. Solutions of different pH values based on a citrate buffer (pH 2-6) or on a HEPES buffer (pH 6.5-8.5) were mixed with 200 μM CG. Absorbance of CG in each solution was done on a Cary 50 Bio UV-Vis spectrophotometer (Agilent Technologies, Santa Clara, CA, USA). The apparent pKa value was obtained from a Boltzmann type equation fit of the absorbance versus pH plot.

Spectrofluorimetry and fluorescence anisotropy

Fluorescence emission spectra and steady state anisotropy measurements were done on a Cary Eclipse fluorescence spectrophotometer (Agilent Technologies, Santa Clara, CA, USA) using 10 μM of fluorescent probes in HB at pH 7.4 with 20 mM Na^+. Fluorescence spectra were blank subtracted and represented as the intensity normalized to the peak value. Anisotropy was calculated according to the following equation:

$$r = \frac{I_{vv} - GI_{vh}}{I_{vv} + 2GI_{vh}}$$

where I_{vv} and I_{vh} are the intensities of fluorescence emission components parallel and perpendicular to the excitation light polarization, respectively, and G a correction factor defined by $G=I_{hv}/I_{hh}$.

Nanoprobe calibration

Calibrations for Na^+, K^+ and pH were done by mixing calibration solutions having known [Na^+], [K^+] and pH values with 10 μM of fluorescent probes. Fluorescence emission spectra were obtained with a Cary Eclipse fluorescence spectrophotometer. Fluorescence intensities of the emission maxima were plotted against known electrolyte concentrations to generate calibration curves. Na^+ calibration was performed as previously described [62] with intracellular-like solutions containing (mM): 165 Na^++K^+, 30 Cl^-, 135 gluconate, 10 HEPES, pH 7.4. K^+ calibration solutions contained (mM): 0-200 K^+, 20 Na^+, 10 HEPES, pH 7.4. Calibration solutions for pH contained (mM): 145 K^+, 20 Na^+, 30 Cl^-, 135 gluconate 10 HEPES, pH 6.5-8.0.

Electron microscopy

PAMAM-PEG-CG nanoparticles were diluted at 1:1000 in water. Formvar-carbon coated EM grids were incubated for 5 minutes floating on a drop of diluted nanoparticles. After a short wash with water they were stained for 2 minutes with 4% (w/v) uranyl acetate in water. The grids were air-dried. Images were taken with a transmission electron microscope (CM100, Philips Electron Optics, now FEI Company, Eindhoven, The Netherlands) operated at 80 keV with a MegaView III camera (Olympus Soft Imaging Solutions GmbH, Münster, Germany). Particle measurements were done with Image J (Rasband, W.S., ImageJ, U. S. National Institutes of Health, Bethesda, MA, USA, http://imagej.nih.gov/ij/, 1997-2011). Eight bits grayscale images were background subtracted with a rolling-ball algorithm, median filtered and automatically thresholded with the maximum entropy method. Particles were automatically analyzed in the resulting binary image after application of a watershed algorithm to separate contiguous particles, using an area criterion of 100-700 px^2. Particles were modeled as ellipses and the particle radius was calculated as the average of minor and major radii.

Brain slice preparation

All experimental procedures were carried out according to the Swiss Ordinance on Animal Experimentation. Sprague-Dawley rats (P14-P23) were decapitated and 300 μm thick transverse slices of somatosensory cortex were cut in cold extracellular solution using a vibrating microslicer (VT1000, Leica Microsystems, Heerbrugg). Slices were incubated at 34°C for 1 hour and then held at room temperature (20–22°C) in extracellular solution until recording.

Single-cell electroporation

The nanoprobe (1 mM) was added to a pipette solution containing (mM): 130 K-gluconate, 5 NaCl, 10 Hepes (adjusted to pH 7.3 with KOH) and loaded in a 4-5 MΩ glass pipette. The pipette was lowered in the slice and approached to the target neuron until close contact was obtained between the membrane and the tip of the pipette. A short (1-10 ms) voltage pulse (10-15 V) was applied to the pipette solution in order to simultaneously expel the fluorescent probe from the pipette and electroporate the cell membrane. Cell loading was monitored with a laser

scanning confocal microscope (see below). Pipette could be moved to different cells in sequence to obtain multi-cell loading.

Fluorescence imaging

Fluorescence acquisitions were done on a LSM 510 Meta laser scanning confocal microscope with a 40x0.8 N.A. water-dipping objective (Carl Zeiss, Jena) using either a 488 nm Argon laser (CG-based probes) or a 543 nm Helium-Neon laser (CR-based probes) for excitation. Fluorescence emission was collected either with a photomultiplier tube or on a spectral detector (Meta detector). To assess the diffusion of the probes in recorded neurons, z-stacks were acquired at 1µm intervals. Three-dimensional reconstructions of these neurons were performed from z-stacks using the Imaris software package (Bitplane, Zurich, Switzerland) and represented in 2D as maximum intensity projections. To monitor the fluorescent baseline stability and measure responses to neuronal stimulations, acquisitions of image time-series were done in frame mode (512x512 pixels) at a rate of 1-2 Hz. Fluorescence intensity over time traces were drawn from regions of interest with Image J (Rasband, W.S., http://imagej.nih.gov/ij/), corrected for background and represented as fractional fluorescence changes over the baseline ($\Delta F/F$) with Igor Pro (Wavemetrics Inc., Portland, OR, USA).

Electrophysiology

Brain slices were continuously superfused at a rate of 2 ml/min with an extracellular solution containing (mM): 125 NaCl, 2.5 KCl, 26 $NaHCO_3$, 1.25 NaH_2PO_4, 2 $CaCl_2$ and 1 $MgCl_2$, 10 glucose, bubbled with 95% O_2 and 5% CO_2. Borosilicate glass pipettes with resistances of 4.0-5.0 MΩ containing (mM): 130 K-gluconate, 5 NaCl, 10 Hepes, 10 phosphocreatine, 2 Mg-ATP, 0.5 Na_2-GTP (adjusted to pH 7.3 with KOH) were used to obtain whole-cell recordings. PAMAM-PEG-CG 10 µM was added to the pipette solution where indicated. Signals were amplified using a Multiclamp 700B amplifier (Molecular Devices, Sunnyvale, CA, USA), filtered at 3 KHz, digitized at 10 KHz using Digidata 1440 (Molecular Devices), and acquired with pClamp 10 electrophysiology package (Molecular devices). In voltage clamp mode, cells were held at -70 mV. For current clamp recording cells were kept with 0 holding current injected. Access resistance and holding current were monitored throughout the experiments, and data were discarded when these parameters increased over 30 MΩ or below -30 pA respectively.

Intrinsic membrane properties were recorded after a settling time of ≥ 10 min. Electrophysiology recordings were analyzed with the pClamp 10 (Molecular Probes).

Neuronal Stimulation

Pharmacological stimulations were done by local application with a glass pipette of tip diameter 1-2 μm, filled with glutamate (200 μM in extracellular solution). The pipette was placed at 10 μm from the soma and pressure pulses of 10-250 ms, 1-2 psi were applied to the back of the pipette with a Pressure System II (The Toohey Company, Fairfield, NJ, USA) to expel the drug. Electrical stimulations were performed using tungsten parallel bipolar electrodes (WPI, Sarasota, FL, USA) placed in cortical layer 4, below the layer 2/3 target neuron. Depolarizing voltage pulses (3-20 V, 100 μs, 1 Hz) were generated with an isolated constant voltage stimulator (DS2A, Digitimer, Letchworth, UK).

Data processing

Numerical data were collected in Excel (Microsoft, Redmond, WA, USA) or Open office (http://www.openoffice.org/) spreadsheets. Plots and curve-fittings and statistical analysis were done with Kaleidapgraph (Synergy Software, Reading, PA, USA) and Origin (OriginLab, Northampton, MA, USA). Representative images were assembled with Image J (Rasband, W.S., http://imagej.nih.gov/ij/). Pairwise comparisons of anisotropy values were done with 2-tailed t-tests. Data are given as average ± s.e.m.

Drugs

Glutamate and AMPA were obtained from Sigma-Aldrich (St Louis, MO), TTX and CNQX from Biotrend (Anawa Trading, Switzerland). They were prepared as stock solutions in water, except CNQX that was prepared in DMSO. Final dilution in experimental solutions was 1/1000.

Acknowledgement

This study was supported by grant #310A0-119827 and 31003A-135720 of the Swiss National Science Foundation to J.Y Chatton. We thank Dr Bruno Humbel, Electron Microscopy Facility, University of Lausanne for his help on performing EM images of the nanoprobe, and Prof. Dirk Fasshauer, University of Lausanne for his help with fluorescence spectrometry.

Supporting Information Available: Free CG and PAMAM-PEG-CG absorbance spectra. This material is available free of charge via the Internet at http://pubs.acs.org.

References

1. Lichtman, J. W.; Conchello, J. A. Fluorescence microscopy. *Nat Methods* **2005**, 2, 910-9.
2. Yuste, R. Fluorescence microscopy today. *Nat Methods* **2005**, 2, 902-4.
3. Taraska, J. W.; Zagotta, W. N. Fluorescence applications in molecular neurobiology. *Neuron* **2010**, 66, 170-89.
4. Helmchen, F.; Denk, W. Deep tissue two-photon microscopy. *Nat Methods* **2005**, 2, 932-40.
5. Grewe, B. F.; Helmchen, F. Optical probing of neuronal ensemble activity. *Curr Opin Neurobiol* **2009**, 19, 520-9.
6. Cannell, M. B.; Cody, S. H. Fluorescent Ion Measurement. In *Handbook of Biological Confocal Microscopy, third edition*; Pawley, J. B., Ed. SpringerScience+Business Media: New York, 2006; pp 736-745.
7. Minta, A.; Tsien, R. Y. Fluorescent indicators for cytosolic sodium. *J Biol Chem* **1989**, 264, 19449-57.
8. Meier, S. D.; Kovalchuk, Y.; Rose, C. R. Properties of the new fluorescent Na^+ indicator CoroNa Green: comparison with SBFI and confocal Na^+ imaging. *J Neurosci Methods* **2006**, 155, 251-9.
9. Jezek, P.; Mahdi, F.; Garlid, K. D. Reconstitution of the beef heart and rat liver mitochondrial K^+/H^+ (Na^+/H^+) antiporter. Quantitation of K^+ transport with the novel fluorescent probe, PBFI. *J Biol Chem* **1990**, 265, 10522-6.
10. Verkman, A. S.; Sellers, M. C.; Chao, A. C.; Leung, T.; Ketcham, R. Synthesis and characterization of improved chloride-sensitive fluorescent indicators for biological applications. *Anal Biochem* **1989**, 178, 355-61.
11. Neher, E.; Augustine, G. J. Calcium gradients and buffers in bovine chromaffin cells. *J Physiol* **1992**, 450, 273-301.
12. Despa, S.; Vecer, J.; Steels, P.; Ameloot, M. Fluorescence lifetime microscopy of the Na^+ indicator Sodium Green in HeLa cells. *Anal Biochem* **2000**, 281, 159-75.
13. Johnson, I. D. Practical Considerations in the Selection and Application of Fluorescent Probes In *Handbook of Biological Confocal Microscopy, third edition*; Pawley, J. B., Ed. SpringerScience+Business Media: New York, 2006; pp 353-367.
14. Mank, M.; Santos, A. F.; Direnberger, S.; Mrsic-Flogel, T. D.; Hofer, S. B.; Stein, V.; Hendel, T.; Reiff, D. F.; Levelt, C.; Borst, A.; Bonhoeffer, T.; Hubener, M.; Griesbeck, O. A genetically encoded calcium indicator for chronic in vivo two-photon imaging. *Nat Methods* **2008**, 5, 805-11.
15. Frommer, W. B.; Davidson, M. W.; Campbell, R. E. Genetically encoded biosensors based on engineered fluorescent proteins. *Chem Soc Rev* **2009**, 38, 2833-41.
16. Han, M.; Gao, X.; Su, J. Z.; Nie, S. Quantum-dot-tagged microbeads for multiplexed optical coding of biomolecules. *Nat Biotechnol* **2001**, 19, 631-5.
17. Park, J. H.; Gu, L.; von Maltzahn, G.; Ruoslahti, E.; Bhatia, S. N.; Sailor, M. J. Biodegradable luminescent porous silicon nanoparticles for in vivo applications. *Nat Mater* **2009**, 8, 331-6.
18. Anilkumar, P.; Wang, X.; Cao, L.; Sahu, S.; Liu, J. H.; Wang, P.; Korch, K.; Tackett Ii, K. N.; Parenzan, A.; Sun, Y. P. Toward quantitatively fluorescent carbon-based "quantum" dots. *Nanoscale* **2011**, Epub.
19. Mohan, N.; Chen, C. S.; Hsieh, H. H.; Wu, Y. C.; Chang, H. C. In vivo imaging and toxicity assessments of fluorescent nanodiamonds in Caenorhabditis elegans. *Nano Lett* **2010**, 10, 3692-9.

20. Welsher, K.; Liu, Z.; Daranciang, D.; Dai, H. Selective probing and imaging of cells with single walled carbon nanotubes as near-infrared fluorescent molecules. *Nano Lett* **2008**, 8, 586-90.
21. Dhanaraj, J.; Jagannathan, R.; Kutty, T. R. N.; Lu, C. H. Photoluminescence Characteristics of Y2O3:Eu3^{+} Nanophosphors Prepared Using Sol-Gel Thermolysis. . *J. Phys. Chem. B* **2001**, 105, 11098-11105.
22. Tong, L.; Cobley, C. M.; Chen, J.; Xia, Y.; Cheng, J. X. Bright three-photon luminescence from gold/silver alloyed nanostructures for bioimaging with negligible photothermal toxicity. *Angew Chem Int Ed Engl* **2010**, 49, 3485-8.
23. Ruedas-Rama, M. J.; Wang, X.; Hall, E. A. A multi-ion particle sensor. *Chem Commun (Camb)* **2007**, 1544-6.
24. Ruedas-Rama, M. J.; Orte, A.; Hall, E. A.; Alvarez-Pez, J. M.; Talavera, E. M. Quantum dot photoluminescence lifetime-based pH nanosensor. *Chem Commun (Camb)* **2011**, 47, 2898-900.
25. Snee, P. T.; Somers, R. C.; Nair, G.; Zimmer, J. P.; Bawendi, M. G.; Nocera, D. G. A ratiometric CdSe/ZnS nanocrystal pH sensor. *J Am Chem Soc* **2006**, 128, 13320-1.
26. Tomasulo, M.; Yildiz, I.; Kaanumalle, S. L.; Raymo, F. M. pH-sensitive ligand for luminescent quantum dots. *Langmuir* **2006**, 22, 10284-90.
27. Dubach, J. M.; Harjes, D. I.; Clark, H. A. Ion-selective nano-optodes incorporating quantum dots. *J Am Chem Soc* **2007**, 129, 8418-9.
28. Dubach, J. M.; Harjes, D. I.; Clark, H. A. Fluorescent ion-selective nanosensors for intracellular analysis with improved lifetime and size. *Nano Lett* **2007**, 7, 1827-31.
29. Dubach, J. M.; Das, S.; Rosenzweig, A.; Clark, H. A. Visualizing sodium dynamics in isolated cardiomyocytes using fluorescent nanosensors. *Proc Natl Acad Sci U S A* **2009**, 106, 16145-50.
30. Brasuel, M.; Kopelman, R.; Kasman, I.; Miller, T. J.; Philbert, M. A. Ion concentrations in live cells from highly selective ion correlation fluorescent nano-sensors for sodium. . *Sensors, 2002. Proceedings of IEEE* **2002**, 1, 288-292.
31. Buck, S. M.; Xu, H.; Brasuel, M.; Philbert, M. A.; Kopelman, R. Nanoscale probes encapsulated by biologically localized embedding (PEBBLEs) for ion sensing and imaging in live cells. *Talanta* **2004**, 63, 41-59.
32. Rivera Gil, P.; Oberdorster, G.; Elder, A.; Puntes, V.; Parak, W. J. Correlating physico-chemical with toxicological properties of nanoparticles: the present and the future. *ACS Nano* **2010**, 4, 5527-31.
33. Grayson, S. M.; Frechet, J. M. Convergent dendrons and dendrimers: from synthesis to applications. *Chem Rev* **2001**, 101, 3819-68.
34. Svenson, S.; Tomalia, D. A. Dendrimers in biomedical applications--reflections on the field. *Adv Drug Deliv Rev* **2005**, 57, 2106-29.
35. Menjoge, A. R.; Kannan, R. M.; Tomalia, D. A. Dendrimer-based drug and imaging conjugates: design considerations for nanomedical applications. *Drug Discov Today* **2010**, 15, 171-85.
36. Jansen, J. F.; de Brabander-van den Berg, E. M.; Meijer, E. W. Encapsulation of guest molecules into a dendritic box. *Science* **1994**, 266, 1226-9.
37. Kline, K. K.; Morgan, E. J.; Norton, L. K.; Tucker, S. A. Encapsulation and quantification of multiple dye guests in unmodified poly(amidoamine) dendrimers as a function of generation. *Talanta* **2009**, 78, 1489-91.

38. Tomalia, D. A.; Frechet, J. M. Discovery of Dendrimers and Dendritic Polymers: A Brief Historical Perspective. *J. Polym. Sci.: Part A: Polym. Chem.* **2002**, 40, 2719-2728.
39. Wangler, C.; Moldenhauer, G.; Saffrich, R.; Knapp, E. M.; Beijer, B.; Schnolzer, M.; Wangler, B.; Eisenhut, M.; Haberkorn, U.; Mier, W. PAMAM structure-based multifunctional fluorescent conjugates for improved fluorescent labelling of biomacromolecules. *Chemistry* **2008**, 14, 8116-30.
40. Jansen, J. F.; Meijer, E. W. Bengal rose@dendritic box. *Macromol. Symp.* **1996**, 102, 27-33.
41. Baars, M. W.; Kleppinger, R.; Koch, M. H.; Yeu, S. L.; Meijer, E. W. The Localization of Guests in Water-Soluble Oligoethyleneoxy-Modified Poly(propylene imine) Dendrimers. *Angew Chem Int Ed Engl* **2000**, 39, 1285-1288.
42. Baars, M. W.; Meijer, E. W. Host-Guest Chemistry of Dendritic Molecules. In *Topics in Current Chemistry: Dendrimers II*; Vögtle, F., Ed. Springer Berlin / Heidelberg, 2000; Vol. 210, pp 131-182.
43. Leisner, D.; Imae, T. Polyelectrolyte Behavior of an Interpolyelectrolyte Complex Formed in Aqueous Solution of a Charged Dendrimer and Sodium Poly(l-glutamate). *The Journal of Physical Chemistry B* **2003**, 107, 13158-13167.
44. El-Sayed, M.; Kiani, M. F.; Naimark, M. D.; Hikal, A. H.; Ghandehari, H. Extravasation of poly(amidoamine) (PAMAM) dendrimers across microvascular network endothelium. *Pharm Res* **2001**, 18, 23-8.
45. Domanski, D. M.; Klajnert, B.; Bryszewska, M. Incorporation of fluorescent probes into PAMAM dendrimers. *Bioelectrochemistry* **2004**, 63, 193-7.
46. Arun, K. T.; Jayaram, D. T.; Avirah, R. R.; Ramaiah, D. beta-Cyclodextrin as a photosensitizer carrier: effect on photophysical properties and chemical reactivity of squaraine dyes. *J Phys Chem B* **2011**, 115, 7122-8.
47. Imhof, A.; Megens, M.; Engelberts, J. J.; de Lang, D. T. N.; Sprik, R.; Vos, W. L. Spectroscopy of Fluorescein (FITC) Dyed Colloidal Silica Spheres. *The Journal of Physical Chemistry B* **1999**, 103, 1408-1415.
48. Riedinger, A.; Zhang, F.; Dommershausen, F.; Rocker, C.; Brandholt, S.; Nienhaus, G. U.; Koert, U.; Parak, W. J. Ratiometric optical sensing of chloride ions with organic fluorophore-gold nanoparticle hybrids: a systematic study of design parameters and surface charge effects. *Small* **2010**, 6, 2590-7.
49. Balzani, V.; Ceroni, P.; Gestermann, S.; Gorka, M.; Kauffmann, C.; Vogtle, F. Fluorescent guests hosted in fluorescent dendrimers. *Tetrahedron* **2002**, 58, 629-637.
50. Zhang, F.; Ali, Z.; Amin, F.; Feltz, A.; Oheim, M.; Parak, W. J. Ion and pH sensing with colloidal nanoparticles: influence of surface charge on sensing and colloidal properties. *Chemphyschem* **2010**, 11, 730-5.
51. Nevian, T.; Helmchen, F. Calcium indicator loading of neurons using single-cell electroporation. *Pflugers Arch* **2007**, 454, 675-88.
52. Fleidervish, I. A.; Lasser-Ross, N.; Gutnick, M. J.; Ross, W. N. Na^+ imaging reveals little difference in action potential-evoked Na^+ influx between axon and soma. *Nat Neurosci* **2010**, 13, 852-60.
53. Fritzinger, B.; Scheler, U. Scaling behaviour of PAMAM dendrimers determined by diffusion NMR. *Macromol. Chem. Phys.* **2005**, 206, 1288–1291.
54. Hedden, R. C.; Bauer, B. J. Structure and Dimensions of PAMAM/PEG Dendrimer-Star Polymers. *Macromolecules* **2003**, 36, 1829-1835.

55. Prosa, T. J.; Bauer, B. J.; Amis, E. J. From Stars to Spheres: A SAXS Analysis of Dilute Dendrimer Solutions. *Macromolecules* **2001**, 34, 4897-4906.
56. Tomalia, D. A.; Naylor, A. M.; Goddard, W. A. Starburst Dendrimers: Molecular-Level Control of Size, Shape, Surface Chemistry, Topology, and Flexibility from Atoms to Macroscopic Matter. *Angewandte Chemie International Edition in English* **1990**, 29, 138-175.
57. Yang, H.; Lopina, S. T.; DiPersio, L. P.; Schmidt, S. P. Stealth dendrimers for drug delivery: correlation between PEGylation, cytocompatibility, and drug payload. *J Mater Sci Mater Med* **2008**, 19, 1991-7.
58. Kim, Y.; Klutz, A. M.; Jacobson, K. A. Systematic investigation of polyamidoamine dendrimers surface-modified with poly(ethylene glycol) for drug delivery applications: synthesis, characterization, and evaluation of cytotoxicity. *Bioconjug Chem* **2008**, 19, 1660-72.
59. Maiti, P. K.; Çağın, T.; Lin, S.-T.; Goddard, W. A. Effect of Solvent and pH on the Structure of PAMAM Dendrimers. *Macromolecules* **2005**, 38, 979-991.
60. Kang, J.; Arcuino, G.; Nedergaard, M. Calcium Imaging of Identified Astrocytes in Hippocampal Slices. In *Imaging in neuroscience and development: a laboratory manual*; Yuste, R.; Konnerth, A., Eds; Cold Spring Harbor Laboratory Press: Cold Spring Harbor, 2005; pp 290-297.
61. Szmacinski, H.; Lakowicz, J. R. Sodium Green as a potential probe for intracellular sodium imaging based on fluorescence lifetime. *Anal Biochem* **1997**, 250, 131-8.
62. Rose, C. R.; Ransom, B. R. Intracellular sodium homeostasis in rat hippocampal astrocytes. *J Physiol* **1996**, 491 (Pt 2), 291-305.

Table 1. *Intrinsic membrane properties*

Property	Control (n=10)	PAMAM-PEG-CG (n=4)
V_m, *mV*	–73.7 ± 1.8	–70.5 ± 1.7
R_{in}, *MΩ*	270.0 ± 48.7	260.9 ± 51.2
AP		
Amplitude, mV	74.1± 2.4	71.9 ± 2.9
HW, ms	2.4 ± 0.2	2.4 ± 0.1
Threshold, mV	–39.8 ± 0.8	–40.8 ± 1.1
AHP		
Amplitude, mV	12.0 ± 1.4	10.2 ± 1.8
HW, ms	136.7 ± 7.4	139.1 ± 33.9
F-I slope, Hz/nA	97.0 ± 20.1	95.7 ± 10.3

Values are means ± s.e.m. R_{in}, input resistance; V_m, resting membrane potential; AP, action potential; AHP, afterhyperpolarization; HW, width at half maximum; F-I, frequency-intensity curve. Significance: comparison between columns with 2-tailed unpaired t-tests did not find any significant difference.

Figure legends

Figure 1. Dendrimer-based sodium-sensitive fluorescent nanoprobes. (A) Sketch representing the idealized principle of a nanoprobe composed of a G5 PAMAM-PEG dendrimer with Na^+ dye CoroNa Green encapsulated in one of the cavities (green). Tertiary amines (in blue) are thought to play an important role in the dye encapsulation. Estimated size: 6.5 nm, estimated molecular mass: 104 kDa. (B) Fluorescence emission spectra of CoroNa Green (λ_{ex} 495 nm), CoroNa Red (λ_{ex} 556 nm) and derived PAMAM-based nanoprobes.

Figure 2. Sodium dependency and selectivity of nanoprobes. (A) Emission spectra of PAMAM-PEG-CG measured at different Na^+ concentrations (λ_{ex} 495nm). (B) Na^+ calibration curves of CoroNa Green and the 3 nanoprobes. Colored lines are linear fits to the respective calibration values (n=9). Data are percent fluorescence changes from 0 mM [Na^+] ± s.e.m. (C,D) Calibration curves for K^+ and for pH, respectively, performed in the presence of 20 mM Na^+. Data are percent fluorescence changes from 0 mM [K^+] and pH 6.5, respectively, ± s.e.m (n=9).

Figure 3. Cell loading with a sodium-sensing nanoprobe. (A) Fluorescent image of cortical pyramidal neurons loaded with PAMAM-PEG-CG superimposed to a differential interference contrast (DIC) image of the brain slice. The pipette used for loading the nanoprobe appears on the right side of the larger neuron. (B) Maximum intensity projection of a 3D confocal image stack acquired through a neuron loaded with PAMAM-PEG-CG. (C) Multi-cell loading of neighboring neurons. (D) Representative time-courses of baseline fluorescence in neurons loaded with free CoroNa Green or PAMAM-PEG-CG. Scale bars, 10 μm.

Figure 4. TEM image of PAMAM-PEG-CG nanoprobe positively stained with 4% uranyl acetate. Nanoparticles appear as dark circular elements due to the uptake of the contrast agent. Scale bar, 50 nm.

Figure 5. Time-lapse measurements of sodium responses in neurons loaded with PAMAM-PEG-CG. (A) Fluorescent signals measured in neuronal cell body during short local application of neurotransmitter glutamate and inhibition by the AMPA receptor blocker CNQX (20 μM).

Numbers of glutamate puffs are indicated below traces. (B) Average response to pharmacological stimulation with glutamate. Data are averages ± s.e.m. (n=3 cells). Red line is the linear fit to the data (R^2=0.993). (C) Single-trial fluorescence transients measured in neuronal cell body during electrical stimulation of afferent nerve fibers. The number of stimulation pulses is indicated below traces. (D) Individual responses to electrical stimulations as a function of pulse number (n=3 cells). Red line is the linear fit to the data (R^2=0.761). (E) Fluorescent signals measured in dendrites during electrical stimulation (upper row) and their inhibition by the Na^+ channel blocker TTX (1μM, lower row).

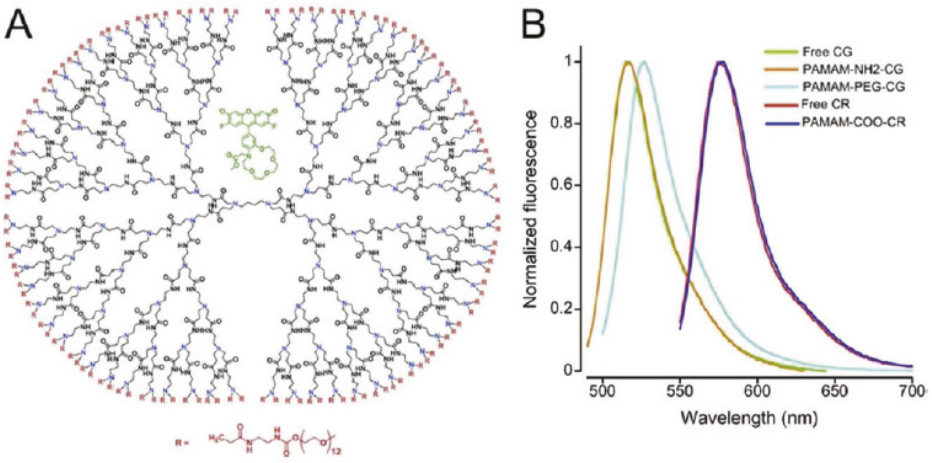
A
B
Free CG
PAMAM-NH2-CG
PAMAM-PEG-CG
Free CR
PAMAM-COO-CR
Normalized fluorescence
Wavelength (nm)
0
0.2
0.4
0.6
0.8
1
500
550
600
650
700

Figure 1

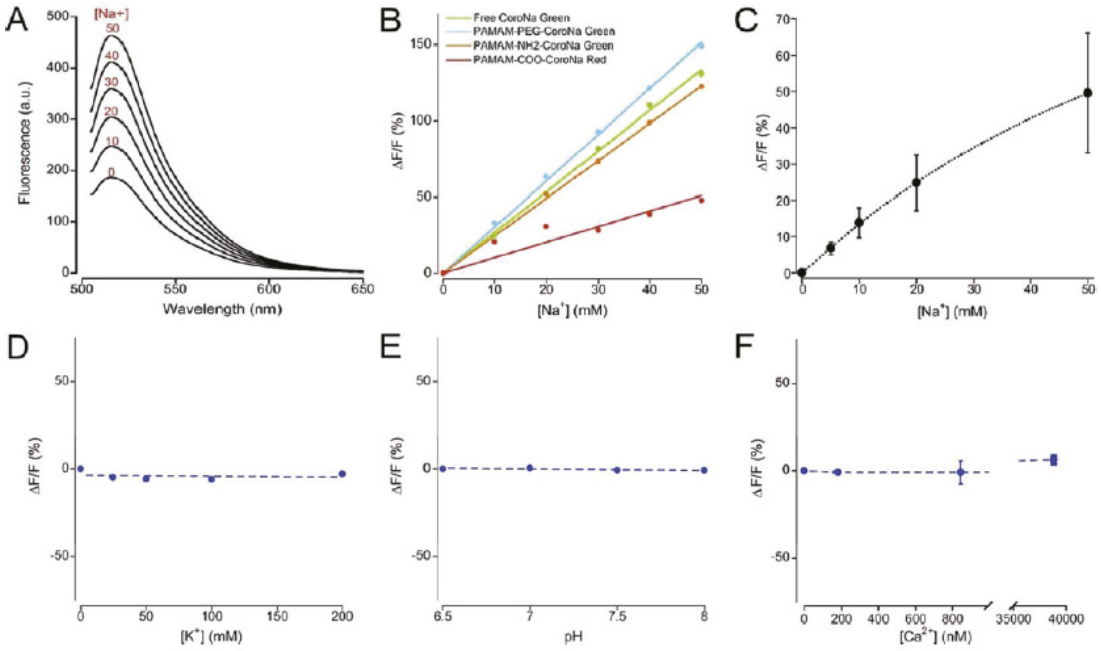
A
[Na+]
50
40
30
20
10
0
Fluorescence (a.u.)
Wavelength (nm)
B
Free CoroNa Green
PAMAM-PEG-CoroNa Green
PAMAM-NH2-CoroNa Green
PAMAM-COO-CoroNa Red
ΔF/F (%)
[Na+] (mM)
C
ΔF/F (%)
[Na+] (mM)
D
ΔF/F (%)
[K+] (mM)
E
ΔF/F (%)
pH
F
ΔF/F (%)
[Ca2+] (nM)

Figure 2

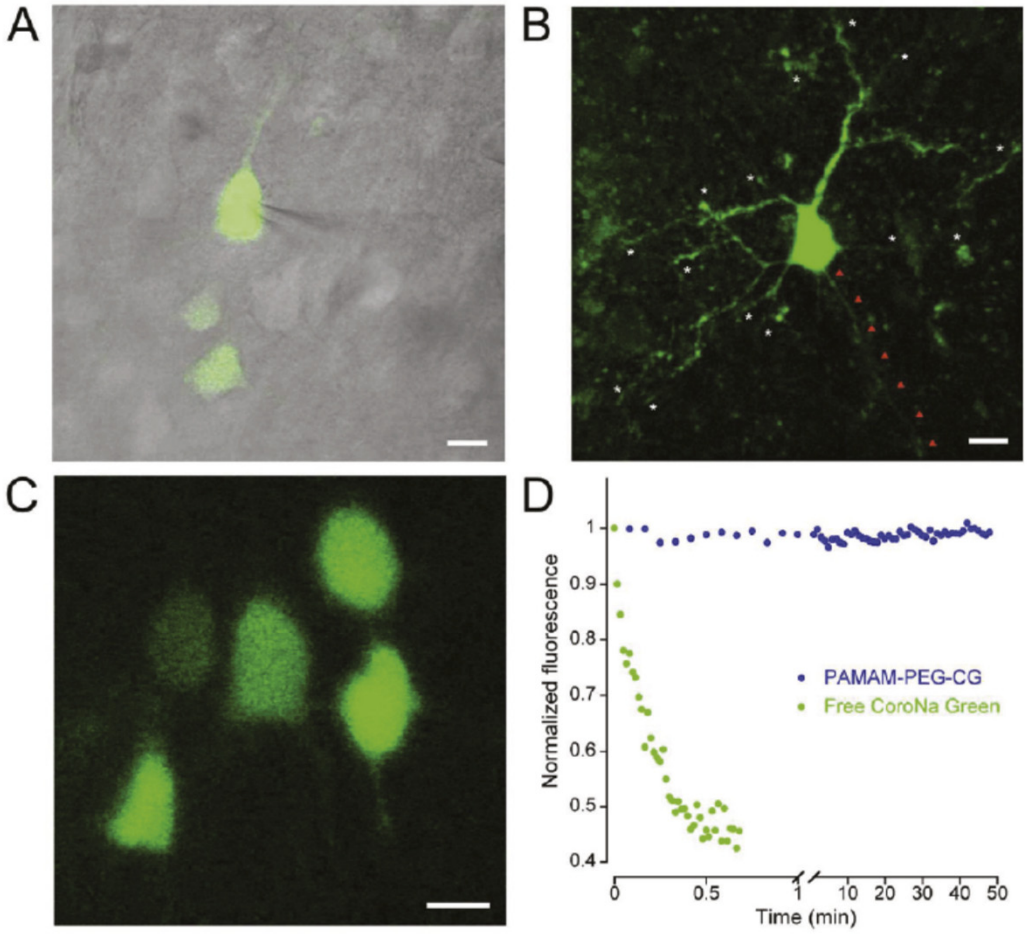
A
B
C
D
Normalized fluorescence
1
0.9
0.8
0.7
0.6
0.5
0.4
PAMAM-PEG-CG
Free CoroNa Green
0
0.5
1
10
20
30
40
50
Time (min)

Figure 3

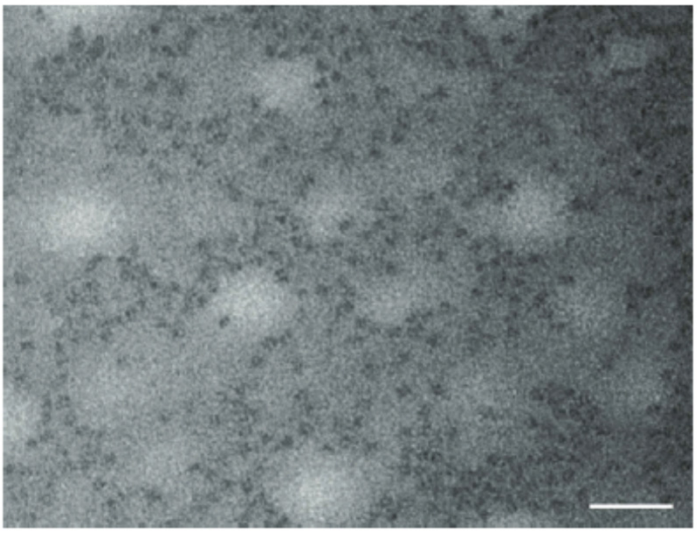

Figure 4

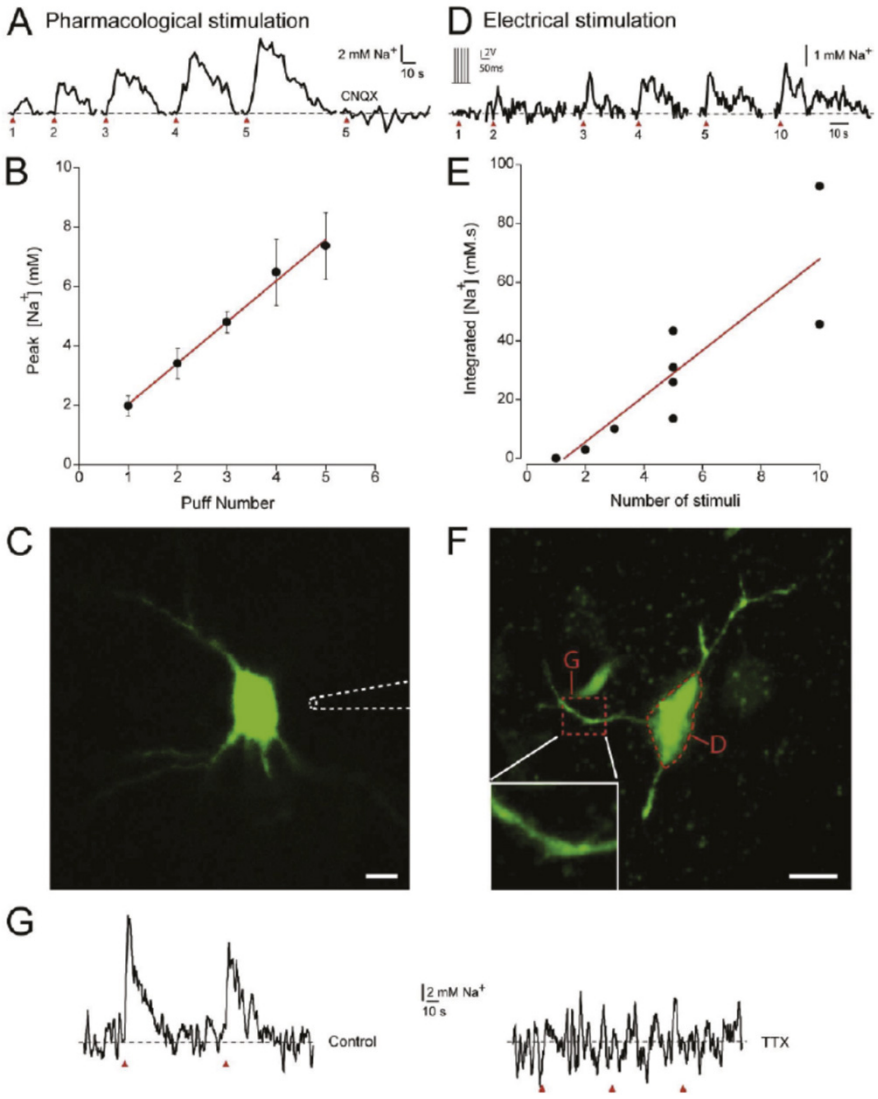
A Pharmacological stimulation
2 mM Na+
10 s
CNQX
1 2 3 4 5 6
D Electrical stimulation
2V
50ms
1 mM Na+
1 2 3 4 5 10
10 s
B
Peak [Na+] (mM)
Puff Number
E
Integrated [Na+] (mM.s)
Number of stimuli
C
F
G
D
G Control
2 mM Na+
10 s
TTX

Figure 5

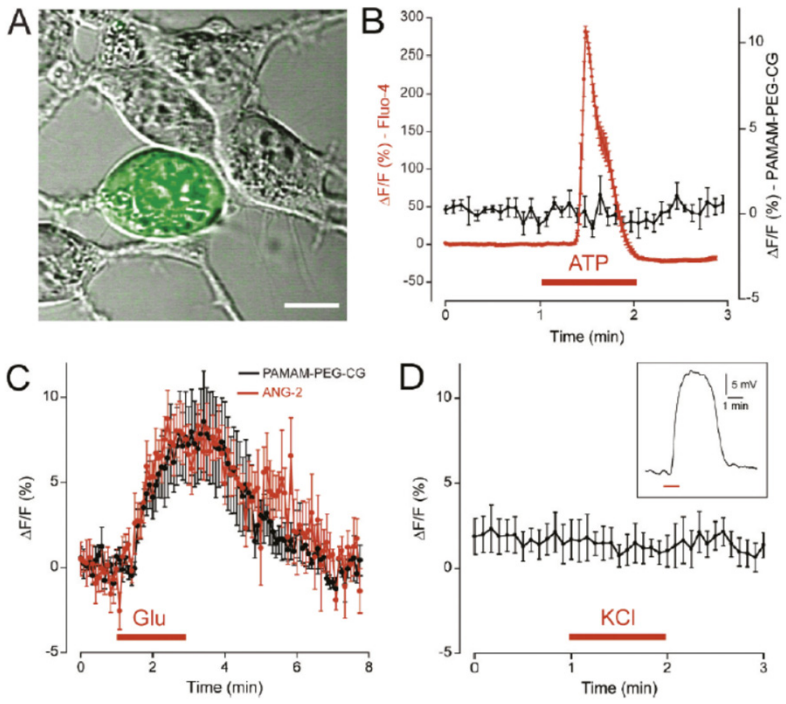
A
B
ΔF/F (%) - Fluo-4
ΔF/F (%) - PAMAM-PEG-CG
ATP
Time (min)
C
PAMAM-PEG-CG
ANG-2
ΔF/F (%)
Glu
Time (min)
D
5 mV
1 min
ΔF/F (%)
KCl
Time (min)

Figure 6